IEEE/CSC & ESAS European Superconductivity News Forum (ESNF), No. 6, October 2008
(ASC Preprint 2LPA03 conforming to IEEE Policy on Electronic Dissemination, Section 8.1.9)

The published version of this manuscript appeared in *IEEE Transactions on Applied Superconductivity* **19**, No. 3, Part 2, 1106 - 1111 (2009)

Fabrication and Test of a 3.7 m Long Support Structure for the LARP Nb_3Sn Quadrupole Magnet LQS01

P. Ferracin, G. Ambrosio, M. Anerella, B. Bingham, R. Bossert, S. Caspi, D. W. Cheng, H. Felice, A. R. Hafalia, C. R. Hannaford, F. Nobrega, S. Prestemon, G. L. Sabbi, J. Schmalzle, F. Trillaud, P. Wanderer, A.V. Zlobin

***Abstract*—The 3.7 m long quadrupole magnet LQS01 represents a major step of the US LHC Accelerator Research Program (LARP) towards the development of long Nb_3Sn accelerator quadrupole magnets for a LHC Luminosity upgrade. The magnet support structure is a scale up of the 1 m long Technology Quadrupole TQS design with some modifications suggested by TQS model test results. It includes an aluminum shell pre-tensioned over iron yokes using pressurized bladders and locking keys (bladder and key technology). The axial support is provided by two stainless steel end plates compressed against the coil ends by four stainless steel rods. The structure, instrumented with strain gauges, has been fabricated and assembled around four aluminum "dummy coils" to determine pre-load homogeneity and mechanical characteristics during cool-down. After presenting the main magnetic and mechanical parameters of LQS01, we report in this paper on the design, assembly, and test of the support structure, with a comparison between strain gauges data and 3D finite element model results.**

***Index Terms*— LARP, Nb_3Sn, Quadrupole magnet**

I. INTRODUCTION

As part of the LHC Accelerator Research Program (LARP [1], [2]), three US national laboratories (BNL, FNAL, and LBNL) are developing the 3.7 m Long Quadrupole magnet LQS01, which represents a fundamental step toward the development of Nb_3Sn magnets for a future LHC IR upgrade. LQS will incorporate four cosϑ-type coils fabricated at BNL and FNAL [3]-[5], and it will be tested in a shell-based support structure designed, fabricated, and assembled at LBNL. Shell-based support structures have been originally developed by the LBNL Superconducting Magnet Program to cope with the needs of high field Nb_3Sn magnets [6]-[8].

Manuscript received 19 August 2008. This work was supported by the Director, Office of Energy Research, Office of High Energy and Nuclear Physics, High Energy Physics Division, U. S. Department of Energy, under Contract No. DE-AC02-05CH11231.

P. Ferracin, B. Bingham, S. Caspi, D. W. Cheng, H. Felice, A. R. Hafalia, C. R. Hannaford, S. Prestemon, G. L. Sabbi, and F. Trillaud are with Lawrence Berkeley National Lab, Berkeley, CA 94720, USA (phone: 510-486-4630; fax: 510-486-5310; e-mail: pferracin@lbl.gov).

G. Ambrosio, R. Bossert, F. Nobrega, and A.V. Zlobin are with Fermilab National Accelerator Laboratory, Batavia, IL 60510, USA.

M. Anerella, J. Schmalzle, and P. Wanderer are with Brookhaven National Laboratory, Upton, NY 11973-5000, USA.

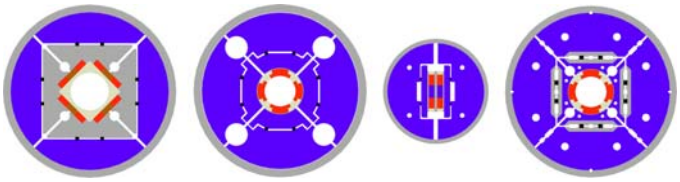

Fig. 1. LARP shell-based (S) magnets (from left to right in chronological order and in scale): Subscale Quadrupole SQ (2004), Technology Quadrupole TQS (2005), Long Racetrack LRS (2006), and Long Quadrupole LQS (under development).

Because of large electro-magnetic forces acting on a brittle superconducting material, these magnets require precise control of the coil pre-load. The main features of shell-based structures are the following: 1) external segmented aluminum shell; 2) iron yoke quadrants separated by open gaps during all magnet operations; 3) assembly attained by joining two sub-assemblies; 4) pre-loading applied with water pressurized bladders; 5) maximum coil stress reached after cool-down; 6) coil ends supported by end-plates and axial rods.

The LQS support structure design relies on the experience gained during the development of several LARP magnets (see Fig. 1). The Sub-scale Quadrupole magnet SQ [9]-[12], tested in 2004, was the first magnet where the shell-based structure was applied to a quadrupole configuration. It used 300 mm long racetrack coils, and included alignment features among all the components. The Technology Quadrupole Shell-based magnet TQS [13]-[19], tested in 2005, applied the concept to 1 m long cosϑ-type coils. Alignment features were not included in the design. In 2006 the Long Racetrack Shell-type magnet LRS [20]-[24] was fabricated and tested: it was the first magnet adopting shell-based structure for long coils, and it implemented two 3.6 m long racetrack coils assembled in a common-coil configuration. The LQS structure is basically an extension of the TQS structure, with some additional features to facilitate assembly and provide alignment of the structural components. The coil-structure alignment, excluded in the LQ magnet design, will be implemented in the High-field Quadrupole magnet HQ [25], [26].

In this paper, we provide a detailed description of LQS01 cable and magnet design in Sec. II. The results of magnetic and mechanical analyses are presented in Sec. III and Sec. IV, while the assembly procedure is discussed in Section V. Finally, Sec. VI describes the cool-down test of a 0.85 m long version of the structure assembled with Al dummy coils.

II. Cable and Magnet Design

LQS01 features the same coil cross-section design as the TQ magnet series, with three conductor blocks wound around titanium alloy pole pieces. The strand and cable design parameters are given in Table I.

TABLE I Cable Design Parameters

Parameter	Unit	
Strand diameter	mm	0.7
Process		RRP
Stack		54/61
No. strands		27
Cu/Sc ratio		0.89
Cable width (bare)	mm	10.050
Cable inner thickness (bare)	mm	1.172
Cable outer thickness (bare)	mm	1.348
Insulation thickness	mm	0.125
No. turns/quadrant (layer 1)		18
No. turns/quadrant (layer 2)		16

The support structure (see Fig. 2) is comprised of four main components: iron pads, iron master keys, iron yokes, and aluminum outer shell. As a first step in the assembly, the four pads are bolted around the coils, while the yoke pieces are inserted inside the 20 mm thick shell (with an outer diameter of 496 mm) and locked in place by gap keys. The coil-pad sub-assembly is then inserted into the shell-yoke sub-assembly. To provide alignment between the coil-pack and the shell/yoke subassemblies, a set of "master keys" assemblies are incorporated. These master keys are matched and nested into precision-machined features in the load pads and yokes. They include grooves for bladders (used to azimuthally pre-load the structures), a central alignment key, and two load keys (used to lock-in the pre-load), whose position has been optimized to minimize coil stresses during all operations.

Alignment between shell and yoke is provided by four pins, located at the four magnet mid-planes. The pad-yoke alignment is achieved through the master keys, which, because of their trapezoidal shape, are nested into the pad and yoke mating features by the bladder pressure. The alignment between the master keys is provided by a central key.

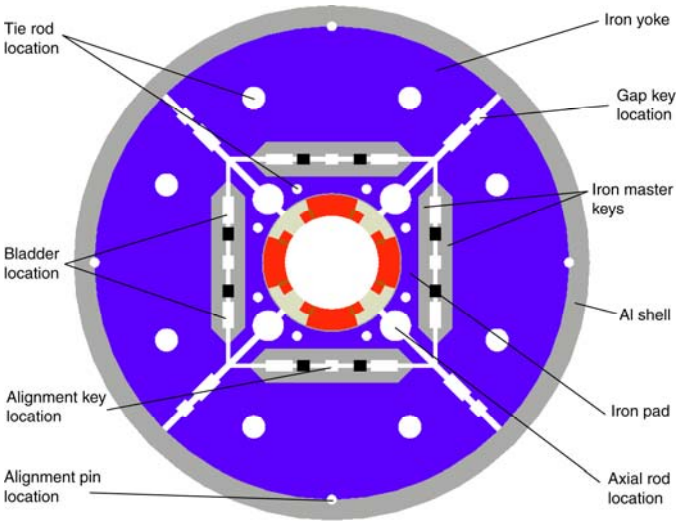

Fig. 2. LQS01 cross-section.

Based on the experience learned from LRS magnet tests [23], [24], in order to improve coil stress homogeneity along the longitudinal axis, the shell has been segmented in four equal-length parts (segments). The 50 mm thick yoke and pad laminations are stacked and pre-compressed by full-length stainless steel tie rods. In order to provide continuous surfaces for the pairs of water pressurized bladders and the load keys, the master keys are machined from 1.7 m long iron plates.

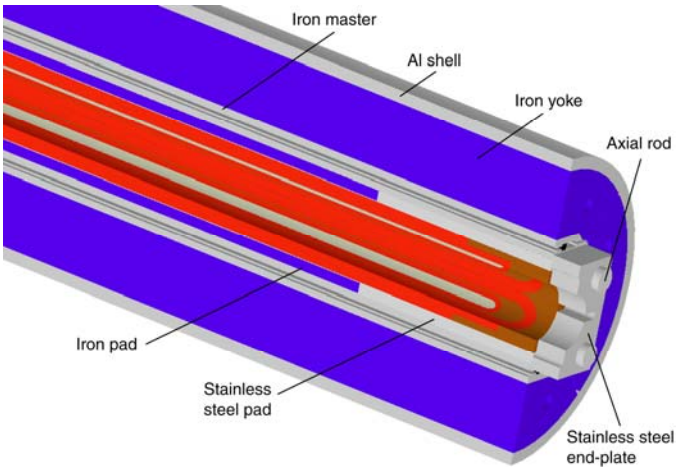

Fig. 3. LQS01 end design.

The coil end support system, similar to the one previously implemented in the HD1 magnet [27], is composed by four stainless steel axial rods, with a diameter of 25.4 mm, inserted in the four clearance holes formed by the bolted pads, and engaged to two 50 mm thick stainless steel end plates (see Fig. 3). With respect to the TQS design, the axial rod locations are closer to the coils to reduce end plate deflections and thickness. The total magnet length is 3.7 m, including end plates and axial rods, while the coil length is 3.4 m.

III. Magnetic Analysis

The field in the conductor has been computed by a 2D finite element magnetic model of the magnet cross-section, where each individual turn has been considered. The assumed critical current density in the superconductor of 2800 A/mm^2 (12 T, 4.2 K) is based on strand measurements for the TQS02 magnet [18], which used the same conductor and heat treatment as the one considered for LQ.

TABLE II Magnetic Design Parameters

Parameter	Unit	4.5 K	4.2 K	1.9 K
Short sample current I_{ss}	kA	13.76	13.96	15.16
Gradient at I_{ss}	T/m	240	244	262
Coil peak field (layer 1) at I_{ss}	T	12.29	12.46	13.43
Coil peak field (layer 2) at I_{ss}	T	10.52	10.66	11.48
Stored energy at I_{ss}	kJ/m	457	479	559
Inductance	mH/m		4.9	

Values computed assuming critical current density in the superconductor of 2800 A/mm^2 (12 T, 4.2 K).

The highest field of 13.4 T (see Table II) at the 1.9 K short sample current is located in layer 1, on the pole turn. The peak field in layer 2, also located in the pole turn, is about 2 T lower then in layer 1. For a field quality analysis performed on the TQ series we refer to [28], [29].

In order to investigate the field in the end and its dependence on the iron design, we analyzed with a 3D magnetic finite element model several cases using different yoke, pad, and master key configurations and materials.

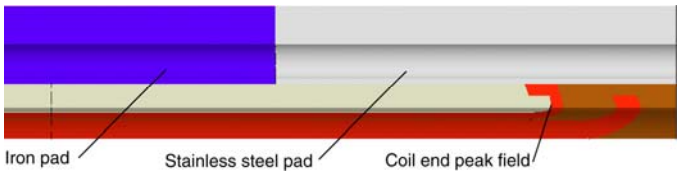

Fig. 4. LQS01 coil end region design.

The final choice is shown in Fig. 4, with stainless steel pads covering the coil end region. In these conditions, the peak field in the end region, which is located in the pole turn of layer 1 (right below the region where the pole turn of layer 2 is bent around the pole) is reduced to the same value as in the straight section.

IV. Mechanical Analysis

A. Cross-section

The stresses in coil and support structure were computed with a 2D finite element mechanical model. The contact surfaces of the impregnated coil (i.e. coil blocks and pole pieces) are assumed bonded, while all the other surfaces are modeled under the assumption of "sliding with separation allowed" with a friction factor of 0.2.

TABLE III Electro-magnetic Forces

	F_x	F_y	F_r	F_θ	F_z
	N/mm	N/mm	N/mm	N/mm	kN
Layer 1	+1673	-1124	+1148	-1503	+17
Layer2	-32	-1039	-311	-1018	+43

Values are computed per octant for a gradient of 240 T/m.

The e.m. forces, listed in Table III, tend to separate the turns from the pole pieces, compressing the coil blocks towards the mid-plane. The shell pre-load is therefore selected so that the contact region between the pole turns and the pole pieces does not exhibit tension larger than 20 MPa (maximum tension that the epoxy is assumed to withstand) when e.m. forces, generated by a gradient of 240 T/m, are applied.

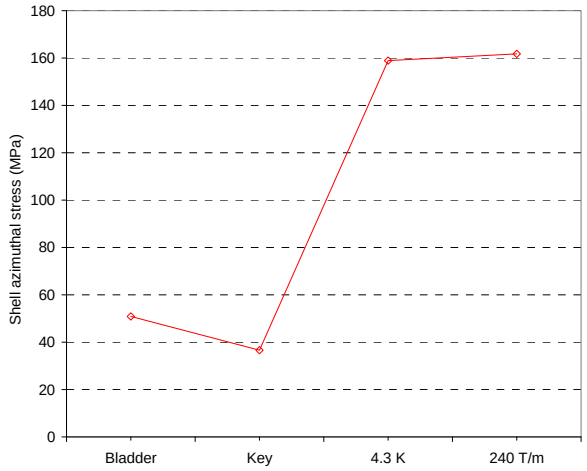

Fig. 5. Computed shell azimuthal stress during bladder operation, after key insertion and bladder deflation, after cool-down, and at 240 T/m.

The computed stresses in shell from assembly to 240 T/m are plotted in Fig. 5. Fig. 6 and Fig. 7 show the stress evolution in the coil layer 1, where the highest values are predicted. The graphs plot the stresses computed for inner, mid and outer radius of the coil, both in the pole turn and mid-plane area.

During bladder operation the shell is pre-tensioned to 51 MPa and the coil compressed to a maximum stress of 99 MPa. Once the load keys are inserted and the bladders deflated, a spring-back is expected in the structure, due to the clearance necessary to slide the load keys between the masters. After cool-down, the shell tension increases to 159 MPa, while the coil pole reaches a peak stress of 139 MPa. As the e.m. forces are applied, the unloading of the coil pole results in a increase of stress on the mid-plane, while marginal variation of shell stress is observed.

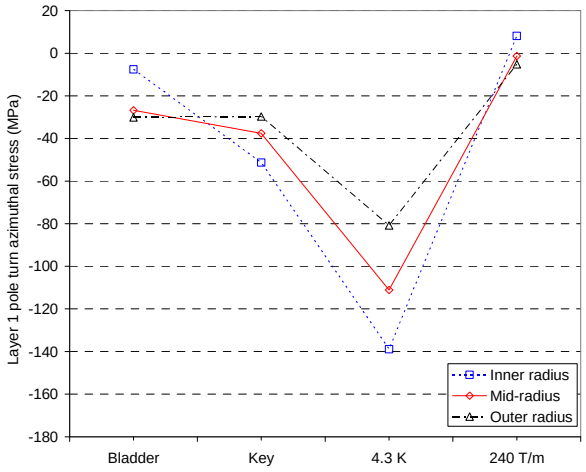

Fig. 6. Computed coil azimuthal stress in layer 1 pole area during bladder operation, after key insertion and bladder deflation, after cool-down, and at 240 T/m.

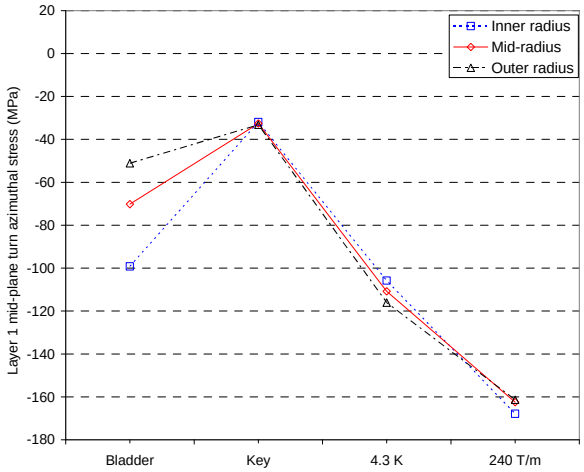

Fig. 7. Computed coil azimuthal stress in layer 1 mid-plane area during bladder operation, after key insertion and bladder deflation, after cool-down and at 240 T/m.

B. End region

The mechanical behavior of the magnet ends was analyzed with a 3D finite element mechanical model, following the integrated modeling technique described in [30]. The longitudinal e.m. forces, which for a 240 T/m gradient amount to 60 kN per octant (see Table III), are directed outwardly, and

they tend to produce gaps between conductors and pole pieces in the end region. Similarly to the approach adopted in the mechanical analysis of the cross-section, the axial pre-load imparted to the coil by the end support has been chosen to minimize the contact tension between coil and end parts when the e.m. forces are applied. According to the model, the contact area between layer 2 pole turn and pole piece in the end region (see Fig. 4) is the more likely to undergo high tension when the magnet is energized. As shown in Fig. 8, the 25.4 mm diameter stainless steel axial rods need to be pre-tensioned at room temperature to 88 MPa, corresponding to 180 kN of total axial force, and they reach after cool-down a tension of 240 MPa, corresponding to 480 kN of total axial force. Such a force compresses the pole turn against the pole piece with a contact pressure of 65 MPa, which reduces to 7 MPa at 240 T/m (see Fig. 9). As observed in the shell, minimum rod stress variations are observed during excitation.

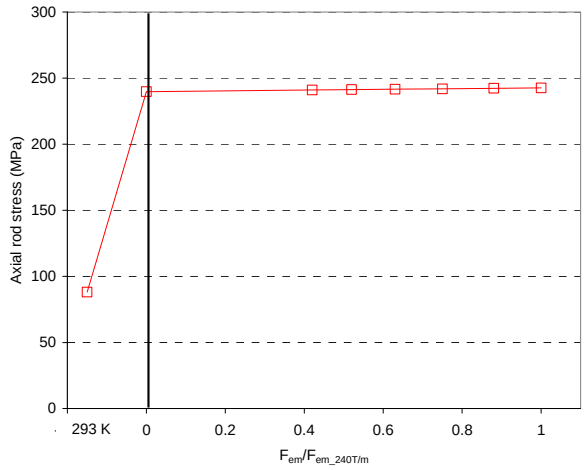

Fig. 8. Axial rod stress after loading at 293 K and as a function of the fraction of e.m. force with respect to the 240 T/m level.

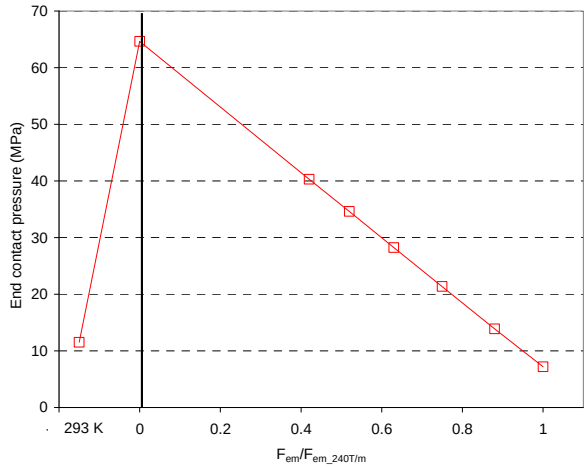

Fig. 9. Contact pressure between layer 2 pole turn and pole piece after loading at 293 K and as a function of the fraction of e.m. force with respect to the 240 T/m level.

V. Assembly Procedure and Tooling

The LQ magnet support structure is composed of four 0.85 m long yoke-shell sub-assemblies, or segments. These segments are individually assembled and pre-loaded, and then combined in a full-length structure.

The assembly procedure for each segment, depicted in Fig.10, starts with the pre-assembly of four 0.85 m long stacks of pad and yoke laminations as shown in Fig. 10a and 10b. The laminations are aligned with bushings and compressed with a hydraulic cylinder, whose force is then locked-in by stainless steel tie-rods and nuts. The yoke-stacks are inserted inside a shell and azimuthally aligned through internal alignment pins (see Fig. 10c) set in precision-machined grooves located in each of the yoke laminations and in the shell inside diameter. In parallel, the pad stacks are bolted around four 0.85 m long aluminum dummy coils (see Fig. 11, left). At this point the coil-pack sub-assembly and the master keys are inserted inside the shell-yoke sub-assembly, and the bladder operation executed. The bladder force pushes the yoke stacks against the shell; once the target shell tension is reached, gap keys are slid in between the yoke stacks (see Fig. 10c), and bladders are deflated. The assembly of the first shell-yoke segment is therefore completed (see Fig. 11, right), and the same operation is repeated for the second segment.

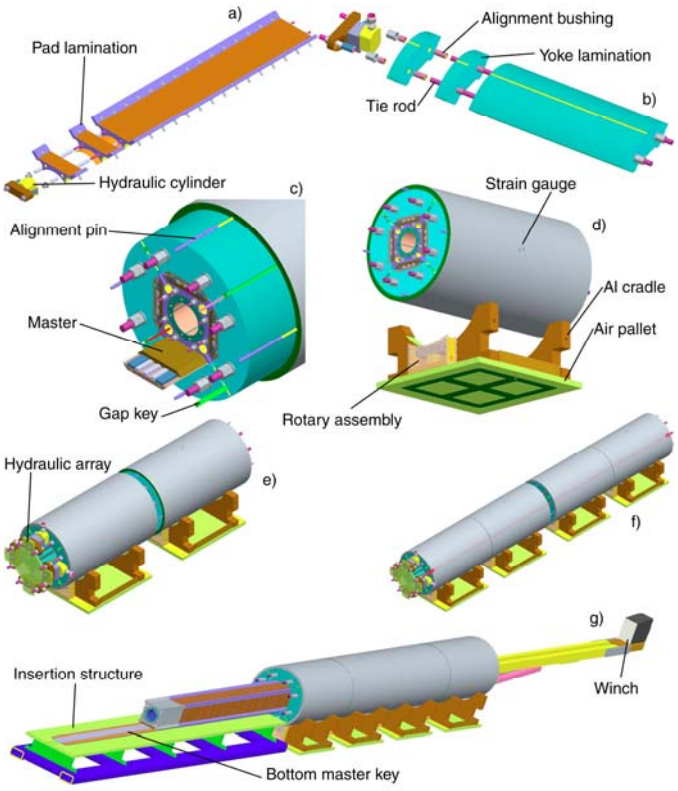

Fig. 10. Assembly steps: pad lamination stacking (a); yoke lamination stacking (b); assembly of first segment (c); segment support system (d); connection of two segments (e); connection of four segments (f); insertion of full-lengh coil-pack.

Each of the segments is then mounted on a specially-designed air support system which facilitate handling and positioning of the two sub-assemblies on a precision granite table. The system is composed by aluminum cradles and rotary assemblies bolted on air pallets (see Fig. 10d). The air pallet is capable of lifting with a cushion of air the full weight of the sub-assembly (about 1 t) at a height of 0.07 mm with respect to the table. The rotary assemblies are designed to hydraulically raise the segments with respect to the cradle and orient them azimuthally to engage the segment-to-segment

alignment pins. After removing the 0.85 m long tie rods, the first two segments, floating on the air pallets, are drawn together with the 1.7 m long tie rods by using a hydraulics array (see Fig. 10e). The tie rod nuts are then torqued and the hydraulics assembly depressurized and removed. The same procedure is used on segments 3 and 4 and for the full-length assembly. As shown in Fig. 10f, the air pallets supporting segments 3 and 4 are activated simultaneously and floated into alignment with the segments 1 and 2. The 3.4 m long yoke tie rods are then inserted and the hydraulics array is used, again, to draw the total assembly together.

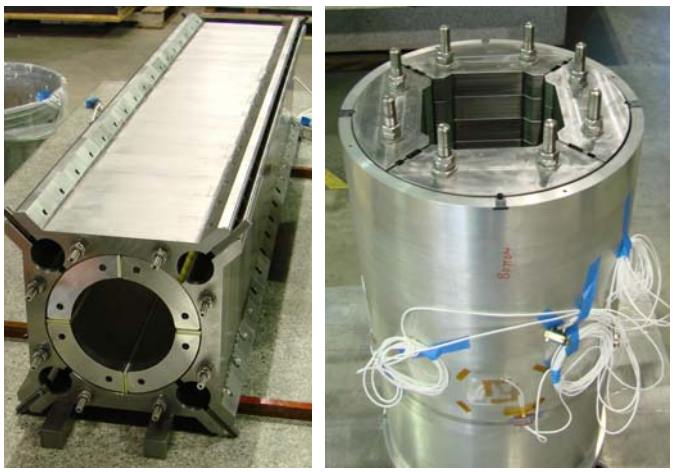

Fig. 11. Section 2 dummy coil–pad sub-assembly (left) and yoke-shell sub-assembly (right) instrumented with strain gauges.

To complete the assembly, the full-length coil pack is placed on a specially designed insertion structure that is accurately positioned in line with the fully assembled shell-yoke sub-assembly (see Fig. 10 g)). The coil-pack sub-assembly is then pulled by a winch in the shell-yoke sub-assembly sliding on the bottom master keys (already installed in the shell/yoke structure). As a last step, the sides and top master keys, the alignment keys, and the bladders are inserted from both ends of the assembly and the azimuthal loading procedure executed.

To axially pre-load the four coils held inside the coil-pack, four 4 m long 25.4 mm diameter stainless steel axial rods are inserted in the clearance cavities created by the assembled coil-pack, and connected to end-plates. A hydraulic cylinder is then installed on the lead ends of the axial rods. As it bears against the end-plate, the hydraulic cylinder simultaneously stretches the axial rods and compresses the coils axially. The force is finally locked by stainless steel nuts.

VI. Cool-down Test

In order to characterize the structure and validate the 3D finite element mechanical model, a 0.85 m long segment (segment 2) of the structure was assembled with four aluminum dummy coils and cooled-down to 77 K. The shell was instrumented with four half-bridge strain gauges placed over the four magnet mid-planes. An identical strain gauge set-up was mounted on the dummy coils. The gauges measured the azimuthal and axial strain at the magnet longitudinal center (see Fig. 10 d)).

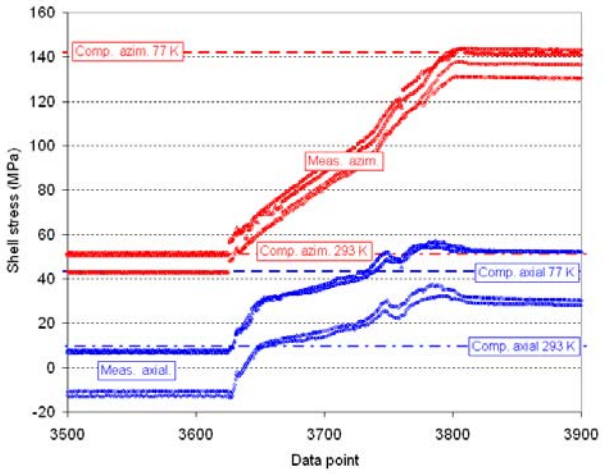

Fig. 12. Gauge measurements of azimuthal and axial stress (MPa) in the shell (markers) and comparison with computed values (dashed lines).

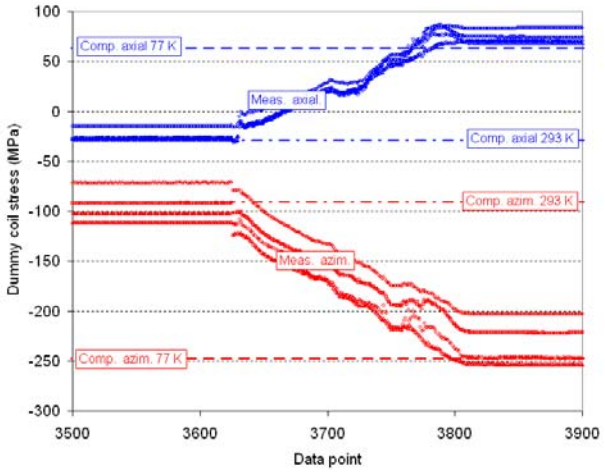

Fig. 13. Gauge measurements of azimuthal and axial stress (MPa) in the dummy coils (markers) and comparison with computed values (dashed lines).

In total, 16 gauges, all thermally compensated by gauges bonded on stress-free aluminum elements, were used to monitor the structure. The measured strain in the azimuthal and axial directions (ε_θ and ε_z) was converted into stress (σ_θ and σ_z) using the relation

$$\sigma_{\theta,z} = \frac{E}{\left(1-\nu^2\right)}\left(\varepsilon_{\theta,z} + \nu\varepsilon_{z,\theta}\right), \qquad (1)$$

where E and ν are, respectively, the elastic modulus (78 GPa at 77 K) and the Poisson's ratio (0.34) of aluminum. The gauge measurements of the shell and dummy coil stress are shown in Fig. 12 and Fig. 13 (markers), and compared with values expected from a 3D finite element model of the segment (dashed lines). At room temperature, the shell was azimuthally pre-tensioned to +47 ± 5 MPa (1 × rms); this resulted in a coil azimuthal pre-compression of -94 ± 17 MPa. After cool-down the shell and coil stress raised to +138 ± 6 MPa and -231 ± 23 MPa respectively. Along the axial direction, the friction with iron yoke and pad, characterized by a lower thermal contraction, prevents the aluminum shell and coil from shrinking, thus generating respectively +41 ± 13 MPa and +74 ± 7 MPa of tension. In both directions, the agreement with the numerical predictions is very good.

VII. Conclusions and Next Steps

The LQS01 magnet will be the first 3.7 m long cosϑ-type quadrupole magnet assembled in a shell-type support structure. The present design of the structure is the result of the experience gained during the development of the LARP SQ, TQS, and LRS magnet series. Additional features have been incorporated to provide alignment between structural components and to facilitate the use of long bladders.

At 4.5 K, LQS01 is expected to generate a gradient of 240 T/m, with a peak field of 12.3 T in the straight section of the layer 1 pole turn. The same peak field is expected in the end region. The structure pre-compresses the coil so that no separation is expected between conductors and pole pieces, both in the straight section and in the ends, once the magnet is energized.

A new assembly procedure, featuring four 0.85 m long segments of the structure pre-assembled individually and then combined together, has been defined. A cool-down test of a 0.85 m long version of the structure assembled around aluminum dummy coils was performed. The strain was monitored with strain gauges mounted on the shell and on the dummy coils. Very good agreement was found between the predictions of a 3D finite element model and strain gauge measurements.

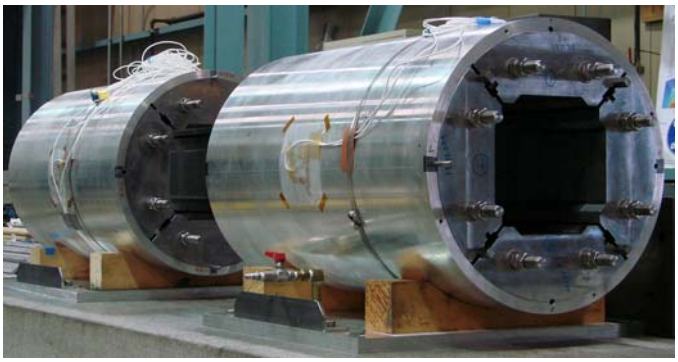

Fig. 14. Pre-loaded segments 1 and 2 on air pallets.

At the time of the submission of this paper, all the components of the structure have been fabricated. Two complete yoke-shell segments (see Fig. 14) have been assembled and the air pallet system has been successfully tested on a segment.

As a next step, the two segments will be connected together with 1.7 m long tie rods. The full assembly and loading of the entire structure with 3.4 m long dummy coils is expected to be completed in the coming months.

References

[1] S. A. Gourlay, *et al.*, "Magnet R&D for the US LHC Accelerator Research Program", *IEEE Trans. Appl. Supercond.*, vol. 16, no. 2, June 2006, pp. 324-327.

[2] P. Wanderer, "Overview for LARP Magnet R&D", presented at *2008 Applied Superconductivity Conference*, Chicago, IL, USA, August 17-22, 2008.

[3] G. Ambrosio, *et al.*, "Design of Nb_3Sn Coils for LARP Long Magnets", *IEEE Trans. Appl. Supercond.*, vol. 17, no. 2, June 2007, pp. 1035-1038.

[4] G. Ambrosio, *et al.*, "LARP Long Nb_3Sn Quadrupole Design", *IEEE Trans. Appl. Supercond*., vol. 18, no. 2, June 2008, pp. 268-272.

[5] G. Ambrosio, *et al.*, "Development of LARP 3.7 m Long Nb_3Sn Quadrupole Models", presented at *2008 Applied Superconductivity Conference*, Chicago, IL, USA, August 17-22, 2008.

[6] S. Caspi, *et al.*, "The use of pressurized bladders for stress control of superconducting magnets", *IEEE Trans. Appl. Supercond*., vol. 11, no. 1, March 2001, pp. 2272-2275.

[7] A. R. Hafalia, *et al*., "A new support structure for high field magnets" *IEEE Trans. Appl. Supercond.*, vol. 12, no. 1, March 2002, pp. 47-50.

[8] A. R. Hafalia, *et al*., "An approach for faster high field magnet technology development", *IEEE Trans. Appl. Supercond.*, vol. 13, no. 2, June 2003, pp. 1258-1261.

[9] P. Ferracin, *et al.*, "Development of a large aperture Nb_3Sn racetrack quadrupole magnet", *IEEE Trans. Appl. Supercond.*, no. 2, June 2005, pp. 1132-1135

[10] P. Ferracin, *et al.*, "Assembly and test of SQ01b, a Nb_3Sn quadrupole magnet for the LHC Accelerator Research Program", *IEEE Trans. Appl. Supercond.*, vol. 16, no. 2, June 2006, pp. 382-385.

[11] P. Ferracin, *et al.*, "Assembly and Tests of SQ02, a Nb_3Sn Racetrack Quadrupole Magnet for LARP", *IEEE Trans. Appl. Supercond*., vol. 17, no. 2, June 2007, pp. 1019-1022.

[12] P. Ferracin, *et al.*, "Effect of Axial Loading on Quench Performance in Nb_3Sn Magnets", *IEEE Trans. Appl. Supercond*., vol. 18, no. 2, June 2008, pp. 285-288.

[13] G. Sabbi, et al., "Nb_3Sn quadrupole magnets for the LHC IR", *IEEE Trans. Appl. Supercond*., vol. 13, no. 2, June 2003, pp. 1262-1265.

[14] S. Caspi, *et al.*, "Mechanical design of a second generation LHC IR quadrupole", *IEEE Trans. Appl. Supercond.*, vol. 14, no. 2, June 2004, pp. 235-238.

[15] A. R. Hafalia, *et al.*, "Structure for an LHC 90 mm Nb_3Sn quadrupole magnet", *IEEE Trans. Appl. Supercond*., vol. 15, no. 2, June 2005, pp. 1444-1447.

[16] S. Caspi, *et al.*, "Design and analysis of TQS01, a 90 mm Nb_3Sn model quadrupole for the LHC luminosity upgrade based on a key and bladder assembly", *IEEE Trans. Appl. Supercond*., vol. 16, no. 2, June 2006, pp. 358-361.

[17] S. Caspi, *et al.*, "Fabrication and Test of TQS01—A 90 mm Nb_3Sn Quadrupole Magnet for LARP", *IEEE Trans. Appl. Supercond*., vol. 17, no. 2, June 2007, pp. 1122-1125.

[18] S. Caspi, *et al.*, "Test and Analysis of Technology Quadrupole Shell (TQS) Magnet Models for LARP", *IEEE Trans. Appl. Supercond*., vol. 18, no. 2, June 2008, pp. 179-183.

[19] S. Caspi, *et al.*, "Test results of LARP Nb_3Sn quadrupole magnets using a shell-based support structure (TQS)", presented at *2008 Applied Superconductivity Conference*, Chicago, IL, USA, August 17-22, 2008.

[20] P. Ferracin, *et al.*, "Design and Fabrication of a Supporting Structure for 3.6 m Long Nb_3Sn Racetrack Coils", *IEEE Trans. Appl. Supercond*., vol. 17, no. 2, June 2007, pp. 1023-1026.

[21] P. Wanderer, *et al*., "LARP Long Nb_3Sn Racetrack Coil Program", *IEEE Trans. Appl. Supercond*., vol. 17, no. 2, June 2007, pp. 1140-1143.

[22] P. Ferracin, *et al.*, "Assembly and Test of a Support Structure for 3.6 m Long Nb_3Sn Racetrack Coils", *IEEE Trans. Appl. Supercond*., vol. 18, no. 2, June 2008, pp. 167-170.

[23] P. Wanderer, *et al.*, "Construction and Test of 3.6 m Nb_3Sn Racetrack Coils for LARP", *IEEE Trans. Appl. Supercond.*, vol. 18, no. 2, June 2008, pp. 171-174.

[24] J. F. Muratore, *et al*., "Test Results of LARP 3.6 m Nb_3Sn Racetrack Coils Supported by Full-Length and Segmented Shell Structures", presented at *2008 Applied Superconductivity Conference*, Chicago, IL, USA, August 17-22, 2008.

[25] H. Felice, *et al*., "Magnetic and Mechanical Analysis of the HQ Model Quadrupole Designs for LARP", *IEEE Trans. Appl. Supercond*., vol. 18, no. 2, June 2008, pp. 281-284.

[26] H. Felice, *et al*., "Design of HQ - a High Field Large Bore Nb_3Sn Quadrupole Magnet for LARP", presented at *2008 Applied Superconductivity Conference*, Chicago, IL, USA, August 17-22, 2008.

[27] A. R. Hafalia, *et al*., "HD1: design and fabrication of a 16 T Nb_3Sn dipole magnet", *IEEE Trans. Appl. Superconduct*., vol. 14, no. 2, June 2004, pp. 283-286.

[28] G. V. Velev, *et al*., "Field Quality Measurements and Analysis of the LARP Technology Quadrupole Models", *IEEE Trans. Appl. Supercond*., vol. 18, no. 2, June 2008, pp. 184-187.

[29] F. Borgnolutti, *et al*., "Reproducibility of the coil positioning in Nb_3Sn magnet models through magnetic measurements", presented at *2008 Applied Superconductivity Conference*, Chicago, IL, USA, August 17-22, 2008.

[30] S. Caspi, and P. Ferracin, "Towards integrated design and modeling of high field accelerator magnets", *IEEE Trans. Appl. Supercond*., vol. 16, no. 2, June 2006, pp. 1298-1303.